Geophysical Journal International

Geophys. J. Int. (2020) **221,** 1341–1348
Advance Access publication 2020 February 19
GJI Seismology

doi: 10.1093/gji/ggaa056

Constraining landslide characteristics with Bayesian inversion of field and seismic data

L. Moretti,[1,2] A. Mangeney,[1,2,3] F. Walter,[4] Y. Capdeville,[5] T. Bodin,[6] E. Stutzmann[1,2] and A. Le Friant[1,2]

[1] *Institut de Physique du Globe de Paris - UMR* 7154, *France*
[2] *Université de Paris, Paris, France*
[3] *INRIA-J. L. Lions, France*
[4] *Laboratory of Hydraulics, Hydrology and Glaciology VAW, ETH Zurich, Switzerland. E-mail: walter@vaw.baug.ethz.ch*
[5] *Laboratoire de Planétologie et Géodynamique de Nantes, F-44300 Nantes, France*
[6] *Univ Lyon, ENS de Lyon, CNRS, UMR* 5276 *LGL-TPE, F-*69622 *Villeurbanne, France*

Accepted 2020 January 27. Received 2019 December 20; in original form 2019 August 20

SUMMARY

Using a fully nonlinear Bayesian approach based on forward modelling of granular flow, we invert for landslide parameters (volume, release geometry and rheology) from different kinds of observations. Synthetic tests show that the runout distance and the deposit area by themselves do not constrain landslide parameters. Better constraints on landslide parameters are obtained from the thickness distribution of the landslide deposits, as well as from the force history applied by the landslide to the ground, which contains information on the landslide dynamics. Therefore, inverting force histories calculated from seismic broad-band records is an important alternative to inverting thickness distributions of landslide deposits, which are usually difficult to obtain. We test the method on the 1997 Boxing Day debris avalanche on Montserrat Island, which involved $40 - 50$ Mm^3. The Bayesian inversion and granular flow model provide good estimates for volume, release geometry and effective friction coefficient. This study thus underlines the value of broad-band seismic records as observations to monitor landslides and validation for their numerical flow models.

Key words: Friction; Geomorphology; Atlantic Ocean; Numerical modelling; Waveform inversion; Volcano seismology.

1 INTRODUCTION

Landslides and avalanches are key erosion processes and represent major natural hazards. Despite important research efforts, the mechanisms that govern flow dynamics and deposition in a natural environment are still unclear. Key questions remain unanswered, such as the origin of the high mobility of some natural flows (e.g. Legros 2002; Iverson *et al.* 2011; Lucas *et al.* 2014).

Numerical granular flow models are an important tool to investigate landslides and avalanches (Delannay *et al.* 2017). However, poor availability of field measurements of flow dynamics makes it difficult to validate these models. Therefore, a common 'inverse approach' is to fit model output to observed landslide characteristics like volume and shape of the released mass, deposit area and runout distance to constrain effective friction, a key underlying rheological parameter (Kelfoun & Druitt 2005; Lucas *et al.* 2011; Pirulli *et al.* 2015).

A problem with the inverse approach is that the thickness distributions of landslide deposits are rarely available as they require digital elevation models (DEMs) immediately before and after the event. Unfortunately, landslide deposits are generally modified by secondary flows or post-event erosion and for landslides terminating in water bodies, deposition DEMs may be nearly impossible to come by. Furthermore, during the stopping phase of granular flows, local surface rearrangements modify the final shape of the deposit, as shown in laboratory experiments (e.g. Farin *et al.* 2014). This rearrangement is difficult to take into account in landslide models. As a result, observed deposits may incorrectly constrain landslide dynamics and rheology. Another key issue is that landslide models may reproduce the deposit even though the simulated dynamics are not correct (e.g. Mangeney-Castelnau *et al.* 2005; Ionescu *et al.* 2015). Therefore, more easily obtainable observations, such as deposit area and runout distance may not be appropriate either.

A range of studies suggests that long-period seismic signals reflecting the history of the force exerted by the landslide mass movement onto the ground may be a better constraint of landslide dynamics (e.g. Kanamori *et al.* 1984; Kawakatsu 1989; Brodsky *et al.* 2003; Favreau *et al.* 2010; Lin *et al.* 2010; Moretti *et al.* 2012; Allstadt *et al.* 2013; Ekström & Stark 2013; Yamada *et al.* 2018; Walter *et al.* 2020). In contrast to static observations of before/after

landscapes, comparing this seismically observed force history with the force simulated by landslide models provides a diagnostic of landslide dynamics. In this way, seismic records can constrain the landslide volume, the number of sub-events and the effect of unusual ground properties, such as glacier ice and erosion processes (Favreau *et al.* 2010; Moretti *et al.* 2012, 2015). Given this perspective, two questions have to be answered: First, how does the inversion of seismically derived force history compare with the inversion of deposit data (runout distance, area of the deposit, spatial distribution of the thickness of the deposit)? Second, what level of constraint can be achieved on landslide parameters (volume, shape of the landslide mass before release, effective friction coefficient, etc.) from inversion of seismic data?

To address these questions we use a Bayesian inversion of synthetic and real data to constrain landslide parameters (volume, 3-D shape of the released mass, effective friction coefficient). We show that runout distance or the deposit area alone cannot constrain these parameters, whereas the force history obtained from seismic data strongly constrains the landslides parameters, nearly as well as the deposit thickness distribution. Our study thus demonstrates that seismic measurements, which are easy to obtain compared to accurate deposition DEMSs, offer a valuable monitoring tool and important insights into landslide dynamics.

2 BAYESIAN INVERSION

We formulate our inversion for landslide parameters in a Bayesian framework (e.g. Sivia & Skilling 2006) where the solution is the expression for the posterior probability density function (PDF) $p(\mathbf{m}|\mathbf{d})$ of our landslide model parameters $\mathbf{m}$ conditioned on observed data $\mathbf{d}$:

$$p(\mathbf{m}|\mathbf{d}) = \frac{p(\mathbf{d}|\mathbf{m}) \times p(\mathbf{m})}{p(\mathbf{d})}, \tag{1}$$

where $p(\mathbf{m})$ is the prior PDF reflecting any knowledge about landslide parameters independent of our observations $\mathbf{d}$ and $p(\mathbf{d}|\mathbf{m})$ is the likelihood function, that is, the probability of making observations $\mathbf{d}$ conditioned by a model $\mathbf{m}$. The PDF of observations $p(\mathbf{d})$ (sometimes referred to as 'evidence') does not depend on model parameters $\mathbf{m}$ and can be determined via normalization of the posterior PDF.

To sample the posterior PDF in eq. (1), we employ the Markov chain Monte Carlo (MCMC) algorithm (Sambridge & Mosegaard 2002; Gallagher *et al.* 2009). We approximate the likelihood function by a multivariate Gaussian PDF:

$$p(\mathbf{d}|\mathbf{m}) = \frac{1}{(2\pi)^{1/2}|\mathbf{V}|^{N/2}} \mathrm{e}^{-\frac{1}{2}((\mathbf{d}-g(\mathbf{m}))^t \mathbf{V}^{-1}(\mathbf{d}-g(\mathbf{m})))}, \tag{2}$$

where $\mathbf{V}$ is the covariance matrix of data errors, $g(\mathbf{m})$ is the forward model prediction for the parameter set $\mathbf{m}$ and N is the number of data points. At each iteration the MCMC algorithm randomly chooses a new model parameter set $\mathbf{m}'$ as a perturbation of the current parameter set $\mathbf{m}$ and calculates an acceptance probability $\alpha = \min(1, p(\mathbf{d}|\mathbf{m}')/p(\mathbf{d}|\mathbf{m}))$. The proposed model $\mathbf{m}'$ is accepted with probability α. If $\alpha = 1$ ($\mathbf{m}'$ gives an equal or higher probability than $\mathbf{m}$), $\mathbf{m}'$ is accepted and becomes the new best parameter set $\mathbf{m}$. Otherwise, a random number u between 0 and 1 is chosen; if $u < \alpha$, the parameter set $\mathbf{m}'$ is accepted, otherwise it is rejected. The MCMC algorithm is designed to generate an ensemble of parameter sets that are distributed according to the posterior distribution. In this way, the posterior PDF can be approximated by a histogram of all the accepted parameter sets. The more iterations we perform the better the approximation to the true posterior PDF $p(\mathbf{m}|\mathbf{d})$.

3 LANDSLIDE MODEL AND PARAMETER SET

To produce model predictions of our landslide parameters, we use the numerical code SHALTOP that simulates landslides over a 3-D topography (Bouchut *et al.* 2003; Bouchut & Westdickenberg 2004; Mangeney *et al.* 2007). SHALTOP is a continuum model based on the depth-averaged thin layer approximation and describes granular flows by taking into account a specific friction law. One example for such a friction law is Coulomb type friction involving a velocity-independent (Savage & Hutter 1989) effective friction coefficient $\mu = \tan\delta$, where δ is the friction angle. Alternatively, variable friction coefficients may be more appropriate as thin layer modelling (such as SHALTOP) of various terrestrial and extraterrestrial landslides has produced evidence for velocity-weakening friction (Lucas *et al.* 2014). Choosing an appropriate friction law and corresponding constant or varying friction coefficients may be challenging and depends on local conditions (Favreau *et al.* 2010).

Given a parameter set $\mathbf{m}$ describing the released mass and the frictional properties, SHALTOP calculates the flow thickness $h(\mathbf{x}, t)$ (where $\mathbf{x}$ is the position vector and t the time), the depth-averaged velocity $\mathbf{u}(\mathbf{x}, t)$ of the granular media and the force $\mathbf{F}(t)$ applied by the landslide to the bed surface (see eqs 4 and 5 in Moretti *et al.* 2015). SHALTOP reliably reproduces laboratory granular flow experiments and real landslides as well as the history of the force inverted from seismic data (Mangeney-Castelnau *et al.* 2005; Favreau *et al.* 2010; Hibert *et al.* 2011; Lucas *et al.* 2011, 2014; Moretti *et al.* 2012, 2015; Yamada *et al.* 2018).

As the main unknowns of the problem, we choose the landslide parameter set $\mathbf{m} = [\delta, h_0, l_0, w_0]$, where δ is the friction angle, h_0, l_0 and w_0, are the thickness, length and width of the initial released mass, respectively (Fig. 1a). In the following, four independent and separate inversions will be carried out to constrain the landslide parameter set. In each case, different data types will be inverted: (1) the runout distance r_f, (2) the area of the deposit $\mathcal{A}_f$, (3) the deposit thickness distribution $h_f(\mathbf{x})$ and (4) the force inverted from seismic data $\mathbf{F}(t)$. The goal is to calculate the *a posteriori* PDF of the parameters and thus to assess which data type best constrains the landslide parameters.

4 INVERSION OF THE CHARACTERISTICS OF A SYNTHETIC GRANULAR FLOW

We first apply the Bayesian approach to synthetic data obtained by simulating a simple granular flow over an inclined plane of inclination angle 10°. A parabolic-shaped mass of thickness $h_0 =$ 30 m, length $l_0 = 200$ m and width $w_0 = 200$ m is released from rest at $t = 0$ s and spreads down the slope until it comes to rest (Figs 1a–c). Simulation of the flow and of the generated force $\mathbf{F}(t)$ is performed using SHALTOP with a friction angle $\delta = 17°$. At each time step the equivalent point source force $\mathbf{F}(t)$ is calculated from the spatial integral of the force field $\mathbf{F}(\mathbf{x}, t)$ applied by the granular mass on the underlying ground.

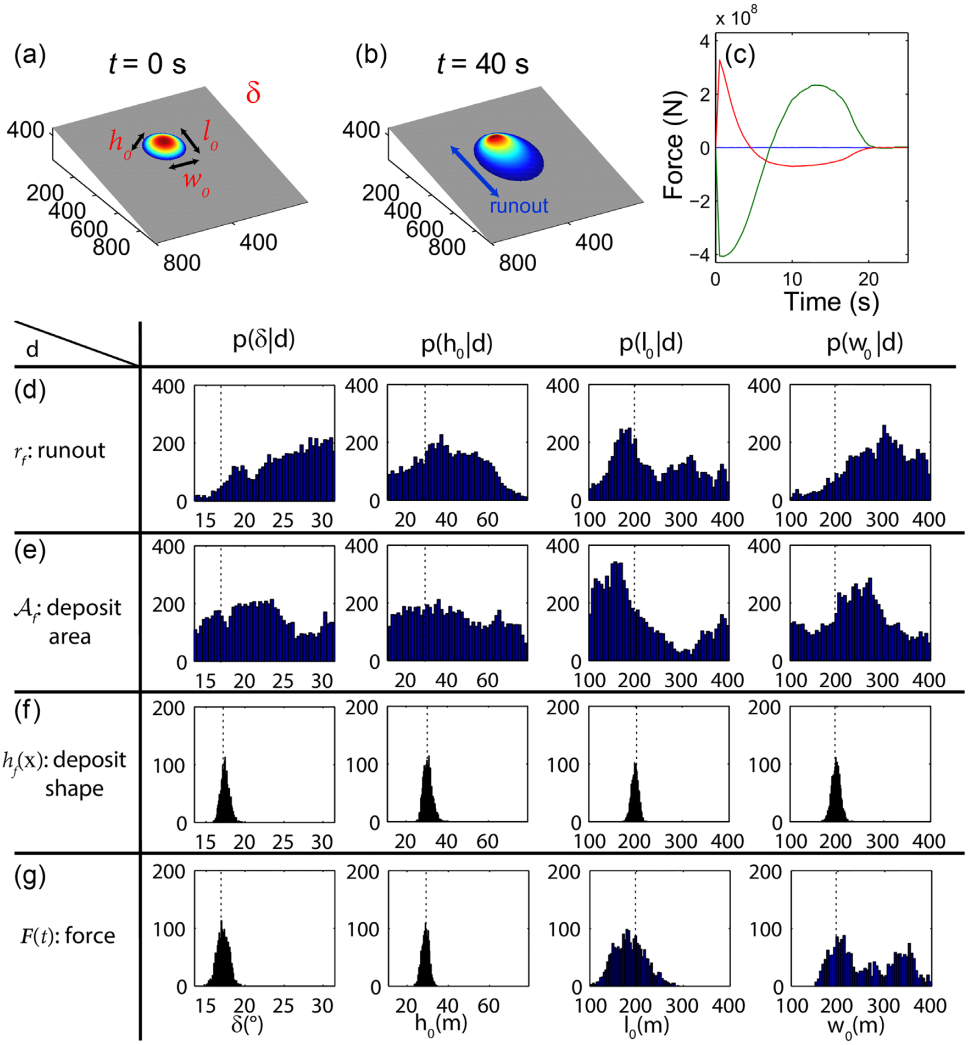

Figure 1. (a) Initial and (b) final shapes of the granular mass simulated using SHALTOP and used as synthetic data for the MCMC inversion [the colours indicate the mass thickness from thin (blue) to 40 m thick (red)], (c) corresponding simulated force applied to the ground surface in the vertical (dashed red), downslope (dotted green) and transverse (solid blue) directions. (d–g) Probability functions of the four parameters δ, h_0, l_0 and w_0 inverted using different data: (d) runout distance r_f, (e) deposit area $\mathcal{A}_f$, (f) deposit shape $h_f(\mathbf{x})$ and (g) force $\mathbf{F}(t)$. The vertical axis of the plots represents the number of accepted parameter sets. The actual values of the parameters (i.e. the input parameters used to simulate the synthetic data) are represented with vertical dotted lines on each plot.

The simulated force in both the downslope and vertical directions reflects the acceleration and deceleration phases of the landslide (e.g., Brodsky *et al.* 2003). As a result of the parabolic mass shape, the force in the transverse direction is symmetric over the longitudinal axis through the mass's centre and thus integrates to zero. Consequently, the transverse spreading is not constrained by the equivalent point source force $\mathbf{F}(t)$. The presence of a more complex topography would provide a non-zero transverse force that would contain information on the transverse spreading dynamics (e.g. Moretti *et al.* 2015).

We assign a flat PDF to the prior $p(\mathbf{m})$, which means that we do not consider prior information on δ, h_0, l_0, and w_0 other than their possible ranges shown in Figs 1(d)–(g). We furthermore assume a diagonal covariance matrix for data errors, which means that the multiple data points of the deposit thickness distribution and force history are not correlated. The assumed measurement uncertainties are typical values for deposit and runout mapping, digital elevation models and inverted forces (Table 1).

Table 1. Uncertainties for synthetic landslide measurements. Spatial uncertainties correspond to grid sizes of simulations and digital elevation models, force history uncertainties are *ca.* 5 per cent of the maximum value (Fig. 1c).

Parameter	Symbol	Uncertainty
Runout distance	r_f	60 m
Deposit area	$\mathcal{A}_f$	4×10^3 m^2
Force history	$\mathbf{F}(t)$	1.6×10^7 N
Deposit distribution	$h_f(\mathbf{x})$	5 m

4.1 Inversion from deposits data

When implementing the MCMC search we made sure that the Markov chains converged. The width of the proposal distribution was chosen in order to have an optimal acceptance rate in the MCMC search, thus maximizing the speed of convergence. We chose 8000

samples such that adding more samples did not significantly change the form of the ensemble solution.

We first take the runout distance as the data of the Bayesian inversion, that is, $\mathbf{d} = r_f$, and perform the 8000 MCMC iterations, after which the algorithm is expected to provide an ensemble of models representing well enough the posterior distribution. Fig. 1(d) shows that the runout distance is unable to constrain the parameter set: the PDF's of all parameters are wide and do not exhibit clear maxima. While the poorly defined maxima of the PDF of h_0 and l_0 roughly correspond to their real values (vertical dotted lines in Fig. 1), the values of w_0 and of the friction coefficient δ are not recovered at all.

Using the deposit area as data, that is, $\mathbf{d} = \mathcal{A}_f$, does not improve the results (Fig. 1e) but results in worse determination of the initial thickness h_0 and length l_0. Compared to the inversion of the runout distance r_f, the somewhat better estimate of w_0 is expected as the transverse extent of the deposit affects deposit area, which we use as data $\mathcal{A}_f$. The highest number of accepted models are obtained for friction angles closer to the real value of δ but with a rather flat histogram shape and the PDF maximum does not correspond to $\delta = 17°$.

In contrast to using runout distance and deposit area as data, the thickness distribution of the deposit, that is, $\mathbf{d} = h_f(\mathbf{x})$, strongly constrains the parameters' set. The better performance does not come as a surprise because the thickness distribution provides multiple data points as opposed to the single data point of runout and deposit area. All landslide parameters exhibit peaked PDF's (Fig. 1f). These maxima correspond to the real parameter values with an error of less than 3 per cent. Indeed, after 8000 iterations, the inversion gives $\delta = 17.44° \pm 1.11°$, $h_0 = 30.61 \pm 4.35$ m, $l_0 = 198.76 \pm 14.98$ m, $w_0 = 198.12 \pm 18.24$ m (uncertainties are standard deviation).

4.2 Inversion from the force applied to the ground

In the next synthetic test, we used the force simulated by the SHALTOP model as data, that is, $\mathbf{d} = \mathbf{F}(t)$ (Fig. 1c). This force is obtained from inversion of seismic data (see next section) and is usually more easily available than deposit DEM's. To be more realistic, we added random noise with amplitudes up to the expected uncertainty (Table 1), still performing 8000 iterations. Fig. 1(g) shows that three parameters are well constrained: h_0, l_0 and δ. The mass width w_0 is less well constrained, exhibiting two maxima. This was expected from the vanishing transverse force as discussed above. Nevertheless, the maxima of all the parameters correspond to their real values with an error calculated from the probability functions smaller than 7 per cent. The inversion gives $\delta = 17.1° \pm 1.5°$, $h_0 = 28.9 \pm 3.6$ m, $l_0 = 196.0 \pm 67.1$ m and $w_0 = 205.4 \pm 49.0$ m.

The force history $\mathbf{F}(t)$ constitutes an observation time-series, which is much easier to obtain than the detailed thickness distribution of the deposit $h_f(\mathbf{x})$ but still makes it possible to constrain the landslide parameters. In real cases, where the topography is irregular, the transverse force no longer vanishes and therefore will provide more information on the transverse mass spreading (e.g., Moretti *et al.* 2012, 2015).

5 REAL LANDSLIDE CASE: THE 1997 BOXING DAY EVENT, MONTSERRAT

We now apply the Bayesian inversion to the Boxing Day debris avalanche that occurred on Montserrat Island on 1997 December

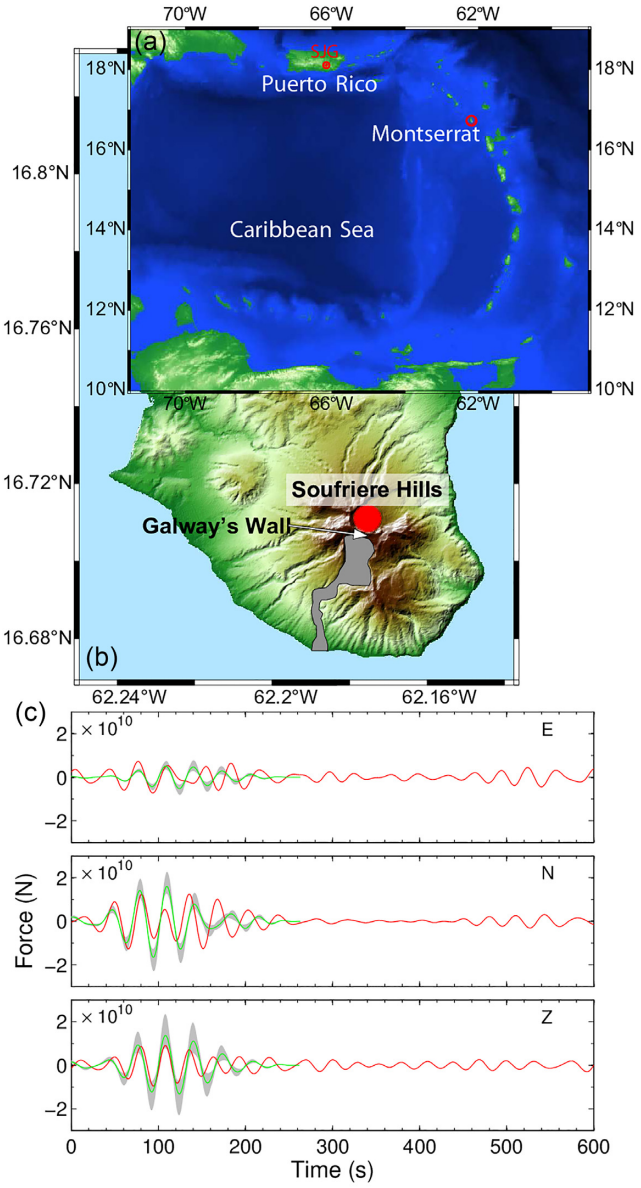

Figure 2. (a) Map of Montserrat Island in the Caribbean Sea. (b) Map of Montserrat Island where the grey area represents the deposits of the Boxing Day debris avalanche within the White River Valley. (c) Force history obtained by waveform inversion of the SJG seismic data (red) and by numerical modelling of the avalanche using the parameters deduced from the Bayesian inversion (green). The grey area represents the 66 per cent confidence interval for the ensemble of parameter sets representing the posterior solution. The forces are filtered in the period range 25-40 s.

26. In this event, the southern flank collapse of the Soufriere Hills Volcano (18.11°N, 66.15°W) generated a debris avalanche with a volume of 40–50 Mm^3 (Heinrich *et al.* 2001; Zhao *et al.* 2014; Fig. 2). We selected this event because (i) it has a simple dynamic history without substantial erosion, motion over a glacier modifying basal fiction (Favreau *et al.* 2010) or multiple subevents, (ii) source area outline and topography before the event are available (Sparks *et al.* 2002).

For the Boxing Day debris avalanche, the three components of $\mathbf{F}(t)$ (Fig. 2c) were obtained by deconvolving the Green's functions from the record at SJG broad-band seismic station (16.71°N,

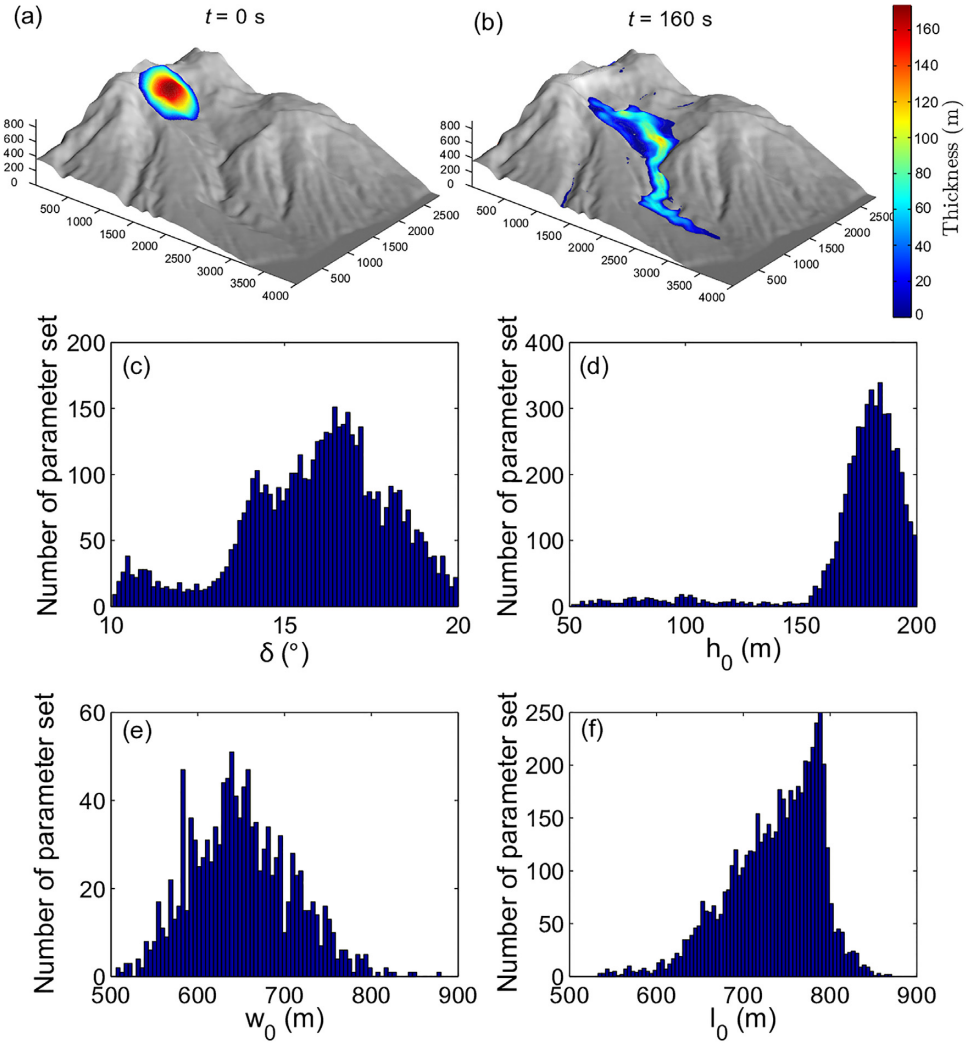

Figure 3. (a) Initial and (b) final states of the simulation using $h_0 = 184$ m, $l_0 = 785.2$ m, $w_0 = 665.6$ m and $\delta = 14.2°$. *A posteriori* probability density of (c) δ, (d) h_0, (e) w_0, and (f) l_0.

62.18°W) located about 448 km away from the Soufriere Hills (Fig. 2a) (Zhao *et al.* 2014). In order to optimize the signal-to-noise ratio, the force was inverted in a rather narrow period range $T \in [25–40]$ s (for details see Zhao *et al.* 2014). Given this frequency range and a landslide motion, which is small compared to the source-station distance of 448 km, the inverted force corresponds to the spatial integral $\mathbf{F}(t)$ calculated with SHALTOP. Finally, Green's functions were calculated using normal modes summation with the 1-D PREM Earth model (Dziewonski & Anderson 1981).

To be on the conservative side, we chose rather high uncertainties for the force history (*ca.* 100 per cent for the east). We compare the simulated and inverted forces rather than the simulated and observed seismic wavefield at the station to facilitate the necessary 8000 simulation runs needed for our Bayesian approach. We acknowledge that our force history is already the result of an inversion, that is linearized and non-Bayesian.

Allstadt *et al.* (2013) and Moretti *et al.* (2015) have previously shown that one-station inversions as used here provide a good estimate of the landslide force history. This has also been shown for seismic signals of iceberg detachment in Greenland (Sergeant *et al.* 2016).

As with the synthetic tests, we approximate the initial collapsing mass by parabolic shape, defined by three parameters: its height h_0, length l_0 and width w_0 (Fig. 3a). Although this is a simplification for a landslide scar, it allows for an efficient Bayesian inversion and at the same time provides an estimate of volume and surface area covered by the released mass. As previously, we use the force history as data (i.e. $\mathbf{d} = \mathbf{F}(t)$) and invert for the landslide parameter set $\mathbf{m} = [\delta, h_0, l_0, w_0]$ and performed 8000 iterations. Note that the seismic signal generated by the force calculated with the best fitting model matches the recorded seismic signal well (Fig. 4). The phase shift between simulated and observed signals on the transverse component may result from uncertainties on Green's functions or approximations made in the flow model.

Figs 3(c)–(f) show that the shape parameters of the collapsing mass h_0, l_0 and w_0 are well constrained as the PDF's exhibit clear maxima. The MCMC algorithm converges toward the values $h_0 = 184 \pm 25.8$ m, $l_0 = 785.2 \pm 57.3$ m, and $w_0 = 665.6 \pm 52.8$ m,

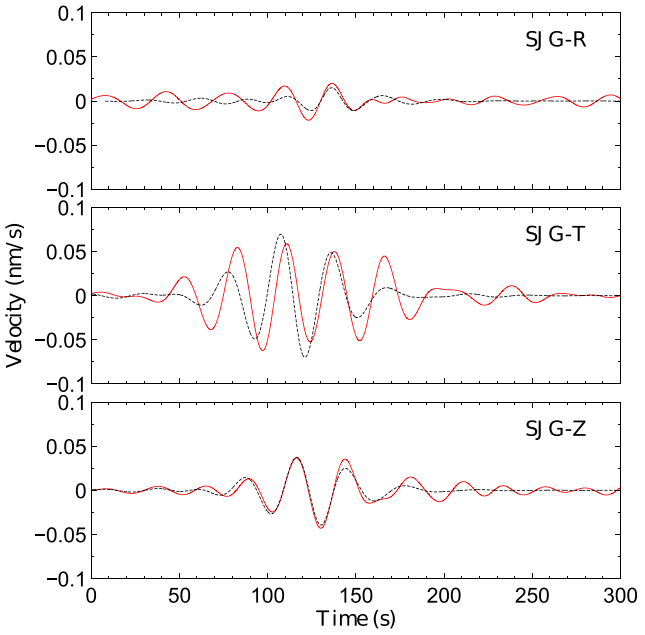

Figure 4. Ground velocity (i.e. seismic signal) calculated by convolution of the force calculated by the best model (i.e. best parameter set) and the Earth Green's functions (dashed black lines), and recorded at SJG seismic station (solid red lines) in the radial, transverse and vertical directions. The signals are filtered between 25 and 40 s.

leading to a volume $V \in [32.7, 58.9]$ Mm^3 with a central value of $V = 45.8$ Mm^3. This is consistent with field observation, which reports a volume of 40–50 Mm^3 and a 400 m wide and 400–500 m long source area with a 100 m high head scarp (Sparks *et al.* 2002; Voight *et al.* 2002). The slightly larger dimensions from our inversion likely reflect the parabolic approximation of the source geometry.

The friction coefficient is not so well constrained and the inversion does not provide a single and well defined solution. Specifically, the PDF exhibits two maxima at $\delta_1 = 14.2^\circ \pm 0.9^\circ$ and $\delta_2 = 16.6^\circ \pm 1.4^\circ$ (Fig. 3c). Using δ_1 underestimates the observed runout distance by only about 150 m while using δ_2 leads to an underestimate by about 800 m. The friction angle $\delta_1 = 14.2^\circ$ is close to the friction angle calibrated by Heinrich *et al.* (2001) to fit the runout distance when using pre-defined field estimates of the dimensions of the collapsing mass. It is also very close to the friction angle deduced from the empirical relation proposed by (Lucas *et al.* 2014), which scales the friction coefficient $\mu = 1/V^{0.0774}$ against the landslide volume V. Indeed, this relation predicts $\mu = 0.26 = \tan(14.34^\circ)$.

Variable friction is a possible explanation for the poor constraint on the effective friction coefficient (Jop *et al.* 2006; Lucas *et al.* 2014; Yamada *et al.* 2018). With the best estimates obtained from the inversion for h_0, l_0 and w_0 (the maxima of the PDFs), we simulated the Boxing Day debris avalanche using (i) a constant friction coefficient (i.e. constant friction angle) $\mu = \tan 14.2^\circ$ and (ii) the variable friction coefficient proposed by Lucas *et al.* (2014) following Rice (2006):

$$\mu(\mathbf{u}) = \mu_w + \frac{\mu_0 - \mu_w}{1 + ||\mathbf{u}||/U_w}, \tag{3}$$

where $\mu_w = \tan 12^\circ$, $\mu_0 = \tan 18^\circ$, $U_w = 4$ m s^{-1} and $\mathbf{u}$ is the local flow velocity. The friction angles 12° and 18° are chosen to represent the variation range of the friction angle around the maxima of the PDF $p(\delta|\mathbf{d})$ (Fig. 5c). Slight changes of these values do not significantly affect the results. The space-averaged friction coefficient is high during the first instants and then decreases towards smaller values (Fig. 5d), as observed in Yamada *et al.* (2018). The simulations for the constant and the variable friction law give comparable deposits (Figs 5a and b). However, some details do improve when taking the variable friction law (3): the runout distance is approximately 200 m longer and thus closer to that observed in the field (Figs 5b and c). Moreover, some details of the thickness distribution $h_f(\mathbf{x})$ such as small bumps before the valley turn near 1500 m north (Fig. 5) are better reproduced with the variable friction coefficient.

6 CONCLUSION

Based on synthetic and real data, we showed that the force history $\mathbf{F}(t)$ that landslides apply to the ground provides a solid constraint for landslide models. Contrary to deposit data, the force history represents a dynamic measurement of the flow, comparable to the velocity field for which observations practically never exist.

We showed that the force history obtained from broad-band seismic records can be inverted using a numerical granular flow model. A fully nonlinear Bayesian inversion makes it possible to recover the initial shape and volume of the released mass together with the effective friction coefficient characterizing the flow. Even though the force history results from a complex mixing of effects related to the initial mass, its shape, landslide trajectory and frictional processes, the granular flow model manages to unravel these effects to provide reliable estimates on landslide parameters. The employed MCMC algorithm gives the posterior PDF and allows us to quantify error estimates of the inverted landslide parameters. Results show that these parameters are quite well constrained.

On the contrary, using the runout distance or the deposit area as data does not allow recovering the initial mass shape and the effective friction. In that case, the PDFs of these parameters are wide and lack clear maxima. While synthetic tests show that the spatial distribution of deposit thickness strongly constrains the Bayesian inversion, such data are often unavailable for natural landslides.

For a real landslide, our Bayesian inversion provides a poorer constraint of the effective friction coefficient compared to the shape and volume of the initial mass. In this case, the PDF of the friction coefficient is wider and exhibits more than one maximum. This likely results from the fact that the effective friction coefficient is not constant during the flow as suggested by granular flow experiments (Jop *et al.* 2006) and by observation of real landslides (Lucas *et al.* 2014). Inversion of other landslides and analysis of high-frequency seismic signals from rockfalls also suggests the signature of variable friction processes in seismic data (Levy *et al.* 2014; Yamada *et al.* 2018).

In conclusion, combining the force history, easily obtained from seismic waveform inversion, with our granular flow model provides a unique tool to back-analyse landslide events. For future applications, the proposed Bayesian approach can leverage this tool to build up a data base of landslide characteristics, including rheological properties.

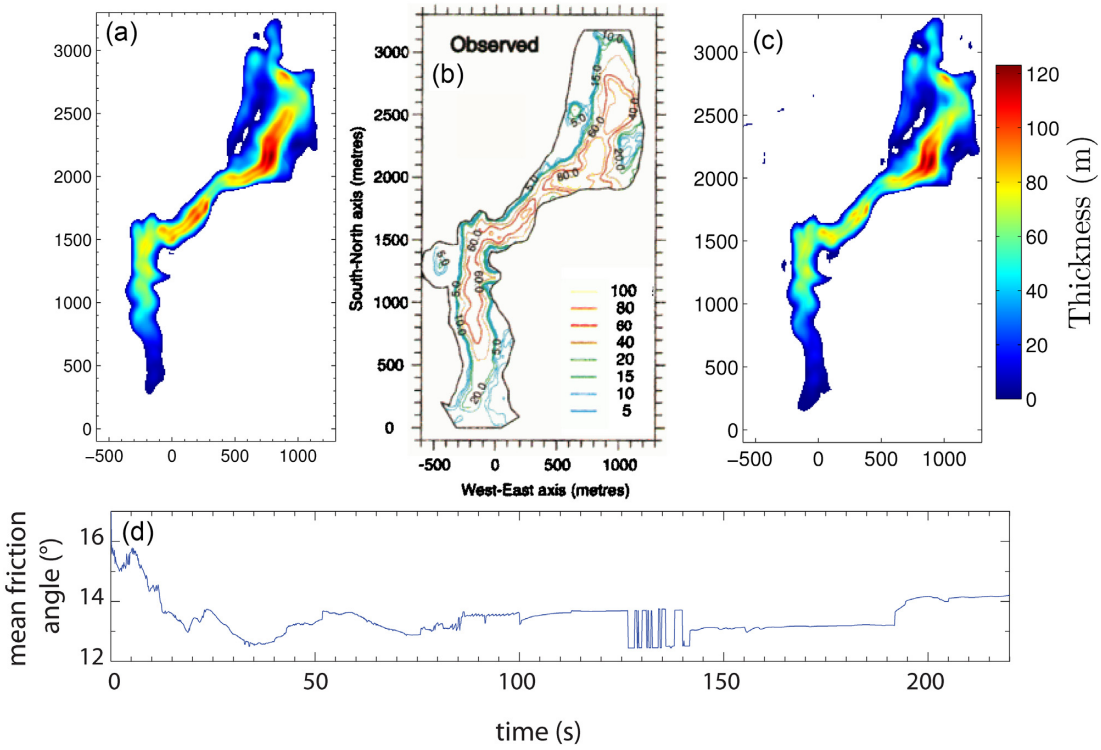

Figure 5. (a) Deposits of the Boxing Day avalanche simulated using a constant friction coefficient ($\delta = 14.2°$), (b) deposit observed in the field extracted from Heinrich *et al.* (2001) and (c) deposits of the simulation using a variable friction coefficient (Lucas *et al.* 2014; see eq. 3). Simulations are performed using the parameters $h_0 = 184$ m, $l_0 = 785.2$ m, $w_0 = 665.6$ m deduced from the Bayesian inversion. (d) Spatially averaged friction angle δ as a function of time for the simulation using the friction law (eq. 3). Note that at the end of the simulation the velocities are not well constrained when deposit height is low because the SHALTOP code calculates fluxes that are divided by flow height to obtain velocities. Consequently, the local friction coefficient is not well constrained at the end of the simulation either.

ACKNOWLEDGEMENTS

We thank Luis Rivera and Jean Paul Montagner for fruitful discussions. This work is supported by ANR-11-BS01-0016 LANDQUAKES, the Seismological and Volcanological Observatories of IPGP and ERC-CG-2013-PE10-617472 SLIDEQUAKE. The salary of FW was paid by the Swiss National Science Foundation via Grants PP00P2_157551 and PP00P2_183719. We thank Göran Ekström and Ianis Gaudot for their constructive reviews that improved the manuscript quality.

REFERENCES

Allstadt, K., 2013. Extracting source characteristics and dynamics of the August 2010 Mount Meager landslide from broadband seismograms, *J. geophys. Res.,* **118,** 1472–1490.

Bouchut, F. & Westdickenberg, M., 2004. Gravity driven shallow water models for arbitrary topography, *Commun. Math. Sci.,* **2,** 359–389.

Bouchut, F., Mangeney-Castelnau, A., Perthame, B. & Vilotte, J. P., 2003. A new model of Saint-Venant and Savage-Hutter type for gravity driven shallow water flows, *C. R. Acad. Sci., Paris I,* **336,** 531–536.

Brodsky, E.E., Gordeev, E. & Kanamori, H., 2003. Landslide basal friction as measured by seismic waves, *Geophys. Res. Lett.,* **30**(24), 2236, doi:10.1029/2003GL018485.

Delannay, R., Valance, A., Mangeney, A., Roche, O. & Richard, P., 2017. Granular and particle-laden flows: from laboratory experiments to field observations, *J. Phys. D: Appl. Phys.,* **50,** 053001, doi:10.1088/1361-6463/50/5/053001.

Dziewonski, A.M. & Anderson, D.L., 1981. PREM is a 1D transversely isotropic, anelastic velocity and density reference model of Earth, *Phys. Earth planet. Inter.,* **25,** 297–356.

Ekström, G. & Stark, C.P., 2013. Simple scaling of catastrophic landslide dynamics, *Science,* **339**(6126), 1416–1419.

Farin, M., Mangeney, A. & Roche, O., 2014. Fundamental changes of granular flow dynamics, deposition, and erosion processes at high slope angles: insights from laboratory experiments, *J. geophys. Res.,* **119**(3), 504–532.

Favreau, P., Mangeney, A.,Lucas,A. Crosta G. & Bouchut, F., 2010. Numerical modeling of landquakes, *Geophys. Res. Lett.,* **37,** L15305, doi:10.1029/2010GL043512.

Gallagher, K., Charvin, K., Nielsen, S., Sambridge, M. & Stephenson, J., 2009. Markov chain Monte Carlo (MCMC) sampling methods to determine optimal models, model resolution and model choice for Earth Science problems, *Mar. Pet. Geol.,* **26**(4), 525–535.

Heinrich, P., Boudon, G., Komorowski, J., Sparks, R., Herd, R. & Voight, B., 2001. Numerical simulation of the December 1997 debris avalanche in Montserrat, Lesser Antilles, *Geophys. Res. Lett,* **28**(13), 2529–2532.

Hibert, C., Mangeney, A., Grandjean, G. & Shapiro, N.M., 2011. Slope instabilities in Dolomieu Crater, La Réunion Island: from seismic signals to rockfall characteristics, *J. geophys. Res.,* **116,** F04032, doi:10.1029/2011JF002038.

Ionescu, I.R., Mangeney, A., Bouchut, F. & Roche, O., 2015. Viscoplastic modelling of granular column collapse with pressure dependent rheology, *J. Non-Newton. Fluid Mech.,* **219,** 1–18.

Iverson, R.M., Reid, M.E., Logan, M., LaHusen, R.G., Godt, J.W. & Griswold, J.P., 2011. Positive feedback and momentum growth during debris-flow entrainment of wet bed sediment, *Nat. Geosci.,* **4,** 116–121.

Jop, P., Forterre, Y. & Pouliquen, O., 2006. A constitutive law for dense granular flows, *Nature,* **441,** 727–730.

Kanamori, H., Given, J.W. & Lay, T., 1984. Analysis of seismic body waves excited by the Mount St. Helens eruption of May 18, 1980, *J. geophys. Res.,* **89**(B3), 1856–1866.

Kawakatsu, H., 1989. Centroid single force inversion of seismic waves generated by landslides, *J. geophys. Res.,* **94**(B9), 12 363–12 374.

Kelfoun, K. & Druitt, T.H., 2005. Numerical modeling of the emplacement of Socompa rock avalanche, Chile, *J. geophys. Res.,* **110,** B12202, doi:10.1029/2005JB003758.

Legros, F., 2002. The mobility of long runout landslides, *Eng. Geol.,* **63,** 301–331.

Levy, C., Mangeney, A., Bonilla, F., Hibert, C., Calder, E.S. & Smith, P.J., 2015. Friction weakening in granular flows deduced from seismic records at the Soufriére Hills Volcano, Montserrat, *J. geophys. Res.,* **120,** 7536–7557.

Lin, C.-H., Kumagai, H., Ando, M. & Shin, T.-C., 2010. Detection of landslides and submarines slumps using broadband seismic networks, *Geophys. Res. Lett.,* **37,** L22309, doi:10.1029/2010GL044685.

Lucas, A., Mangeney, A., Mège, D. & Bouchut, F., 2011. Influence of the scar geometry on landslide dynamics and deposits: application to Martian landslides, *J. geophys. Res.,* **116,** E10001, doi:10.1029/2011JE003803.

Lucas, A., Mangeney, A. & Ampuero, J.P., 2014. Frictional velocity-weakening in landslides on earth and on other planetary bodies, *Nat. Commun.,* **5**(3417), doi:10.1038/ncomms4417.

Mangeney, A., Bouchut, F., Thomas, N., Vilotte, J.P. & Bristeau, M.O., 2007. Numerical modeling of self-channeling granular flows and of their levee-channel deposits, *J. geophys. Res.,* **112,** F02017, doi:10.1029/2006JF000469.

Mangeney-Castelnau, A., Bouchut, F., Vilotte, J.P., Lajeunesse, E., Aubertin, A. & Pirulli, M., 2005. On the use of Saint-Venant equations to simulate the spreading of granular mass, *J. geophys. Res,* **110**(B9), B09103, doi:10.1029/2004JB003161.

Moretti, L., Mangeney, A., Capdeville, Y., Stutzmann, E., Huggel, C., Schneider, D. & Bouchut, F., 2012. Numerical modeling of the Mount Steller landslide flow history and of the generated long period seismic waves, *Geophys. Res. Lett.,* **39**(16), L16402, doi:10.1029/2012GL052511.

Moretti, L., Allstadt, K., Mangeney, A., Capdeville, Y., Stutzmann, E. & Bouchut, F., 2015. Numerical modeling of the mount Meager landslide constrained by its force history derived from seismic data, *J. geophys. Res.,* **120**(4), 2579–2599.

Pirulli, M. & Mangeney, A., 2008. Result of back-analysis of the propagation of rock avalanches as a function of the assumed rheology, *Rock Mech. Rock Eng.,* **41**(1), 59–84.

Rice, R.J., 2006. Heating and weakening of faults during earthquake slip, *J. Geophys. Res.,* **111,** B05311, doi:10.1029/2005JB004006.

Sambridge, M. & Mosegaard, K., 2002. Monte Carlo methods in geophysical inverse problems, *Rev. Geophys.,* **40**(3), 3–1-3-29.

Savage, S.B. & Hutter, K., 1989. The motion of a finite mass of granular material down a rough incline, *J. Fluid Mech.,* **199,** 177–215.

Sergeant, A., Mangeney, A., Stutzmann, E., Montagner, J.P., Walter, F., Moretti, L. & Castelnau, O., 2016. Complex force history of a calving-generated glacial earthquake derived from broadband seismic inversion, *Geophys. Res. Lett.,* **43**(3), 1055–1065.

Sivia, D. & Skilling, J., 2006. *Data Analysis: A Bayesian Tutorial,* Oxford University Press.

Sparks, R. *et al.*, 2002. Generation of a debris avalanche and violent pyroclastic density current on 26 December (Boxing Day) 1997 at Soufriere Hills volcano, Montserrat, *Geol. Soc., Lond., Mem.,* **21**(1), 409–434.

Voight, B. *et al.*, 2002. The 26 December (Boxing Day) 1997 sector collapse and debris avalanche at Soufriere Hills volcano, Montserrat, *Geol. Soc., Lond., Mem.,* **21**(1), 363–407.

Walter, F. *et al.*, 2020. Direct observations of a three million cubic meter rock-slope collapse with almost immediate initiation of ensuing debris flows, *Geomorphology,* **351,** doi.org/10.1016/j.geomorph.2019.106933 .

Yamada, M., Mangeney, A., Matsushi, Y. & Matsuzawai, T., 2018. Estimation of dynamic friction and movement history of large landslides, *Landslides,* **15**(10), 1963–1974.

Zhao, J. *et al.*, 2014. Model space exploration for determining landslide source history from long-period seismic data, *Pure appl. Geophys.,* **172**(2), 389–413.